Nonzero orbital moment in high coercivity ϵ-Fe$_2$O$_3$ and low-temperature collapse of the magnetocrystalline anisotropy

Yuan-Chieh Tseng,[1,2] Narcizo M. Souza-Neto,[2] Daniel Haskel,[2,*] Martí Gich,[3,†] Carlos Frontera,[4] Anna Roig,[4,‡]
Michel van Veenendaal,[2,5] and Josep Nogués[6]

[1]*Department of Materials Science and Engineering, Northwestern University, Evanston, Illinois 60201, USA*
[2]*Advanced Photon Source, Argonne National Laboratory, Argonne, Illinois 60439, USA*
[3]*Saint-Gobain Recherche, 93303 Aubervilliers, France*
[4]*Institut de Ciència de Materials de Barcelona (ICMAB-CSIC), Campus de la UAB, 08193 Bellaterra, Catalunya, Spain*
[5]*Department of Physics, Northern Illinois University, De Kalb, Illinois 60115, USA*
[6]*Institució Catalana de Recerca i Estudis Avançats (ICREA) and Centre d'Investigació en Nanociència i Nanotecnologia (ICN-CSIC),
Campus de la Universitat Autònoma de Barcelona, 08193 Bellaterra, Catalunya, Spain*

The magnetic properties of ϵ-Fe$_2$O$_3$ nanoparticles are investigated by x-ray magnetic circular dichroism. Sum rules relating the orbital and spin moment in the Fe 3d band to the Fe $L_{2,3}$ absorption cross sections show that the Fe orbital moment (m_{orb}) is considerably high, explaining the origin of the large coercivity of this material at room temperature. Moreover, at $T \sim 110$ K, the collapse of the coercivity (H_c) and the magnetocrystalline anisotropy coincides with a strong reduction of the spin-orbit coupling evidenced by a drastic drop of m_{orb}. The decrease in m_{orb} originates from changes in the electron transfer between Fe and O ions accompanied by significant modifications of some of the Fe-O bond distances. Similarly, the recovery of m_{orb} at lower temperatures mimics the behavior of the Fe-O bond lengths.

PACS number(s): 75.50.−y, 71.70.Ej, 78.20.Ls, 87.64.ku

I. INTRODUCTION

Nanostructured materials have generated great interest due to their intriguing properties which can markedly differ from those of their bulk counterparts. Among these, magnetic nanoparticles[1–4] can be singled out for their numerous potential applications exploiting their unusual and tailorable mechanical, electrical, optical, and magnetic properties stemming partly from large surface to volume ratios.[5–8] Reduced particle size, however, can result in stringent requirements, e.g., in magnetic storage applications where the superparamagnetic limit has to be overcome.[9–12] To circumvent this limitation materials with large coercivity (H_C) are required. The interest in ϵ-Fe$_2$O$_3$, for a long time an unexplored polymorph of Fe (III) oxide,[13–15] has recently been revived thanks to the possibility of synthesizing it in pure form[16,17] and because of its appealing and unusual physical properties. Remarkably, ϵ-Fe$_2$O$_3$ cannot be obtained in bulk form but only synthesized as nanoparticles thanks to its low surface energy.[18] Concerning the magnetic properties, ϵ-Fe$_2$O$_3$ exhibits a moderate anisotropy, $K \sim 5 \cdot 10^6$ erg/cm^3, leading to a large H_C of ~ 20 kOe at room temperature[16–24] which collapses to ~ 0.8 kOe at around 110 K.[22–24] In addition, its magnetic and dielectric properties are coupled.[25] The magnetic softening, accompanied by a decrease in the dielectric constant, has been related to a commensurate to incommensurate magnetic transition and the concomitant decrease in the magnetocrystalline anisotropy.[26] The crystal structure of ϵ-Fe$_2$O$_3$ is noncentrosymmetric ($Pna2_1$, $a = 5.0885$ Å, $b = 8.7802$ Å, and $c = 9.4709$ Å at 200 K) with Fe occupying four distinct crystallographic sites, including one tetrahedral (T_d: Fe$_T$) and three octahedral sites [O_h: one regular (Fe$_{\mathrm{RO}}$) and two distorted (Fe$_{\mathrm{DO1}}$), (Fe$_{\mathrm{DO2}}$)] (Fig. 1 depicts the unit cell). The high-temperature magnetic structure of ϵ-Fe$_2$O$_3$ is

that of a collinear ferrimagnetic material with the Fe^{3+} magnetic moments antiferromagnetically coupled along a. The Fe^{3+} magnetic moments in the (Fe$_{\mathrm{DO1}}$) and (Fe$_{\mathrm{DO2}}$) distorted octahedral sites mutually cancel, and the net magnetization results from the uncompensated magnetic moments of the atoms in tetrahedral (Fe$_T$) and regular octahedral (Fe$_{\mathrm{RO}}$) positions yielding a net magnetization of ~ 0.3 μ_B/Fe^{3+} at room temperature. The transformation between the high-temperature and the low-temperature incommensurate magnetic structures, which accompanies the magnetic softening of ϵ-Fe$_2$O$_3$, takes place in at least three stages between 150 and 80 K. In that region, there are signatures of a second-order structural transition involving changes in the coordination of the (Fe$_{\mathrm{DO1}}$) and (Fe$_T$) sites, occurring simultaneously with (or as a consequence of) the emergence of the incommensurate magnetic order. Below 80 K, ϵ-Fe$_2$O$_3$ presents a
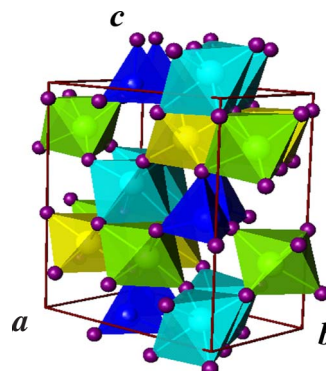

FIG. 1. (Color online) ϵ-Fe$_2$O$_3$ unit cell. The tetrahedral (Fe$_T$) is represented in dark color and three octahedral sites, one regular (Fe$_{\mathrm{RO}}$), and two distorted [(Fe$_{\mathrm{DO1}}$) and (Fe$_{\mathrm{DO2}}$)] are represented in light colors.

square-wave incommensurate magnetic structure.[26] The mechanism behind the large room-temperature coercivity and the low-temperature reduction in magnetic anisotropy has not been elucidated yet. In particular, since transition metal oxides present weak spin-orbit coupling due to the so called orbital quenching,[27] the possible existence of orbital moments in ϵ-Fe_2O_3 was not explored thus far.

In this work, x-ray magnetic circular dichroism (XMCD) experiments were carried out and analyzed within the framework of sum rules.[28–30] XMCD sum rules allow separation of the spin (m_{spin}) and orbital (m_{orb}) components of magnetization. The results show that the effective net spin moment of the ferrimagnetic arrangement of Fe ions, m_{spin}, remains unchanged while at ∼120 K a sudden decrease in effective net orbital moment, m_{orb}, provides unique evidence that changes in orbital magnetization and related changes in spin-orbit coupling are responsible for the coercivity collapse at the transitional temperature range. We argue that at temperatures above 200 K the large m_{orb}/m_{spin} ratio, and thus spin-lattice coupling, is responsible for the large coercivity values and the magnetoelectric behavior found for this iron oxide phase.

II. EXPERIMENTAL

The sample used in the XMCD measurements consists of ϵ-Fe_2O_3 nanoparticles in powder form with an average particle diameter of ∼25 nm. Details of sample preparation can be found in Refs. 17, 22, and 26. The magnetic behavior of ϵ-Fe_2O_3 nanoparticles prepared for the present work was checked to be in accordance with that previously reported in Ref. 22 using a Quantum Design superconducting quantum interference device (SQUID) magnetometer. XMCD measurements were carried out at beamline 4-ID-C of the Advanced Photon Source at Argonne National Laboratory. X-ray absorption spectra (XAS) and XMCD were measured in total electron yield (TEY) and helicity switching mode. XMCD is the difference in XAS data acquired with left- and right-circularly polarized x rays delivered by a circularly polarizing undulator.[31] Measurements were performed at various temperatures (from 20 to 200 K) for two directions of applied magnetic field (±40 kOe) along and opposite the x-ray propagation direction. The temperature dependence of the Fe-O bond length and the cell parameters were obtained from the joint refinement of neutron and x-ray powder diffraction patterns. The diffraction data were, respectively, collected in the D20 instrument at the Institut Laue Langevin (λ=2.42 Å upon heating at 1.7 K/min between 10 and 200 K) and the ID31 diffractometer of european synchrotron radiation facility (ESRF) (λ=0.500 Å at fixed temperatures between 10 and 200 K). The patterns were refined jointly by the Rietveld method using the FULLPROF (Ref. 32) program suite. Mössbauer spectra were acquired at different temperatures between 10 and 300 K using a conventional transmission Mössbauer spectrometer with a ^{57}Co/Rh source. Velocity calibration was done using a 6 μm foil of metallic iron, and the Mössbauer parameters are given relative to this standard at room temperature. The program package NORMOS (Ref. 33) was used to fit the spectra.
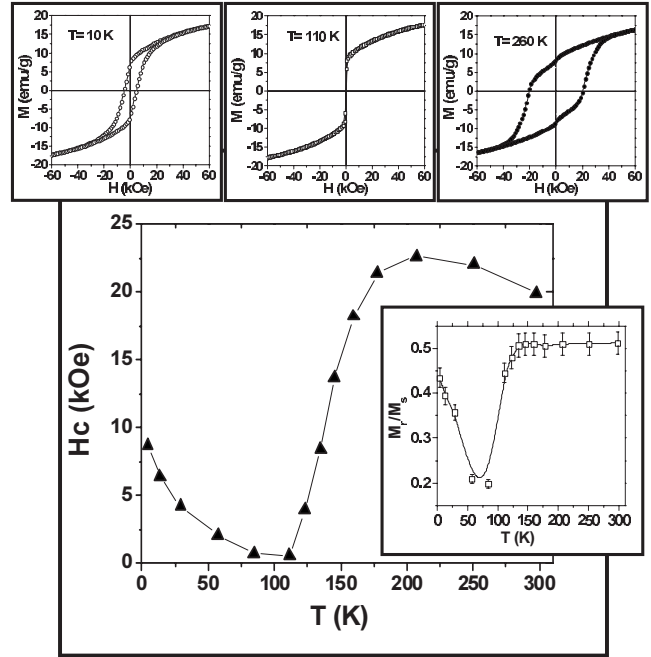

FIG. 2. Temperature dependence of the coercive (H_C) and the squareness ratio M_R/M_S (lower inset) adapted from Ref. 22. The upper insets show the magnetization vs magnetic field hysteresis loops of ϵ-Fe_2O_3 nanoparticles measured at 10, 110, and 260 K.

III. RESULTS AND DISCUSSION

Figure 2 shows the temperature dependence of the coercive field (H_C) and the squareness ratio M_R/M_S (M_R and M_S are remanent and saturation magnetizations, respectively) together with hysteresis loops at selected temperatures. As it is known for this material, H_C at room temperature is rather large H_C (300 K)=20 kOe.[16,22] However, it drastically decreases as the temperature is decreased, reaching a minimum at around 110 K, H_C (110 K)=0.8 kOe. Finally, H_C increases again at lower temperatures;[22] although due to the incommensurate spin arrangement and the concomitant weaker anisotropy, H_C is smaller than the values attained at room temperature. The collapse of coercivity H_C is accompanied by a reduction in M_R/M_s.

Figure 3 shows Fe $L_{2,3}$ XAS and XMCD spectra; the latter shown for opposite applied field directions. Interestingly, the simulated XAS and XMCD line shapes obtained from cluster calculations carried out up to double ligand hole and including contributions from all sites ($1^*T_d+3^*O_h$) are in good agreement with the experimental data as shown in Fig. 3. Since helicity switching is equivalent to magnetization reversal, the XMCD signal is expected to fully reverse upon reversal of applied field. While this is largely observed, data sets for opposite applied fields are not identical. Hence, the sum-rules analysis, described in detail by Chen *et al.*,[30] was carried out separately for the two data sets taken with opposite applied fields to account for systematic errors in the data. The integration ranges and description of parameters entering the sum-rules equation[30] are shown in Fig. 4. The 3*d* electron occupation number, n_{3d}, needed for a quantitative derivation of orbital and spin components of magnetization,
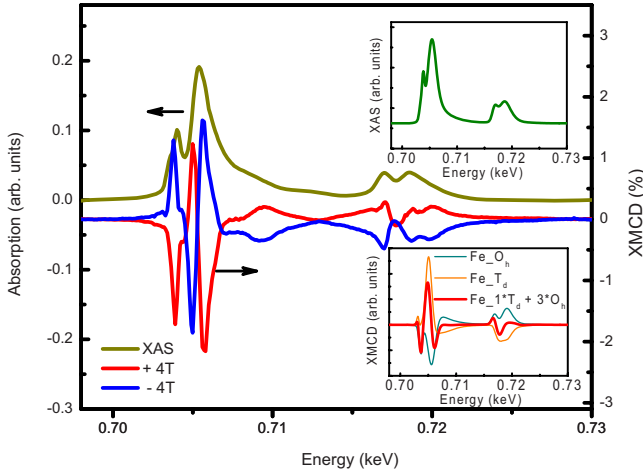
FIG. 3. (Color online) Fe $L_{2,3}$-edge XAS and XMCD upon applied field reversal (± 4 T). Top inset is the simulated XAS. Bottom inset are the simulated XMCD of Fe_{Oh}, Fe_{Td}, and the combined result with $1^*Fe_{Td}+3^*Fe_{Oh}$.

was set to $n_{3d}=5$ based on the $3d^5$ electronic configuration of Fe^{3+} ions. As discussed below, an atomistic description of Fe $3d$ states neglecting d-p mixing is not accurate in this material. In particular, an Fe $3d^5$ configuration carries no net orbital moment (half-filled shell), contrary to the results obtained from the sum-rules analysis. We note that while the derived absolute values of m_{orb} and m_{spin} could be affected by a poorly defined n_{3d}, the m_{orb}/m_{spin} ratio is independent of the $3d$ electron occupation.[30] Cluster calculations (Fig. 3) show that the integrated isotropic absorption[34] for tetrahedral and octahedral Fe sites is within a few percent of one another. This is expected because the strongly overlapping $2p$ and $3d$ wave functions result in similar radial matrix elements for both environments. Furthermore, cluster calcula-
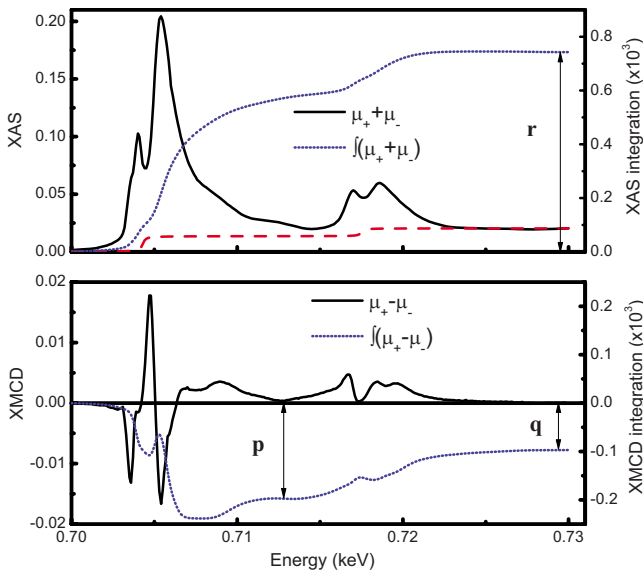

FIG. 4. (Color online) The XAS (top) and XMCD (bottom) integrations (blue lines) applied in sum-rules calculations. $\mu_{+,-}$ are absorption coefficients for opposite photon helicities. r, p, and q are the parameters adopted in sum-rules calculations (Ref. 30).
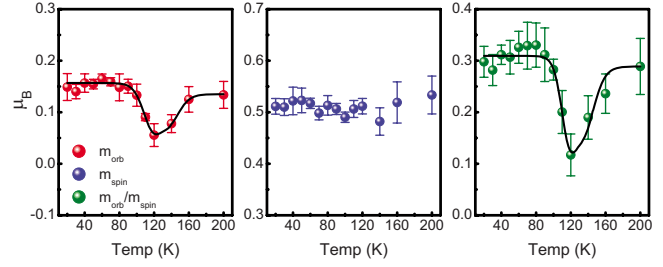

FIG. 5. (Color online) Temperature dependence of the orbital (m_{orb}) (left panel), and spin effective moments (m_{spin}) (middle panel), and the ratio of orbital/spin, (m_{orb}/m_{spin}) (right panel).

tions indicate similar occupancies of 5.6 and 55 electron at the O_h and T_d sites, respectively. Since the sum rules are normalized by the isotropic absorption, this justifies the interpretation in the form of *effective* (averaged over all Fe sites) orbital and spin moments despite the presence of inequivalent Fe sites. Similar arguments have been put forward in Refs. 35 and 36 where inequivalent Fe sites are also present, albeit without theoretical justification. The temperature-dependent m_{orb}, m_{spin}, and m_{orb}/m_{spin} quantities obtained from the sum rules analysis are shown in Fig. 5. At room temperature the derived net magnetic moment $|m_{orb}+m_{spin}| \sim 0.65$ μ_B/Fe is larger than the 0.3 μ_B/Fe obtained from the magnetic and neutron-diffraction measurements at zero field.[22,26] This discrepancy may be due to the very large resonant absorption cross section relative to the absorption edge jump, which results in sum rules being quite sensitive to the details of data normalization and integration. Additionally, the quantitative determination of m_{orb} and m_{spin} can be affected by the substantial overlap of the L_2 and L_3 edges[37] or by the enhanced surface sensitivity in the TEY measurements.[38] Because of these limitations, we focus on the *relative* changes in m_{orb}, m_{spin}, and m_{orb}/m_{spin} with temperature, which are robust since T-dependent data sets underwent identical normalization and integration procedures. Both treatments show that the spin component m_{spin} remains largely temperature independent while the orbital component m_{orb} shows a significant decrease around 120 K. In particular, the m_{orb}/m_{spin} ratio, which is independent of both the $3d$ electron occupation and the integration of XAS data, shows a significant reduction ($>50\%$) in the Fe $3d$ orbital moment at $T \sim 120$ K and subsequently increases to attain at 80 K a value of the same order than the one measured at 200 K. We note that, while changes in relative $3d$ hole occupancy at inequivalent Fe sites are expected in the transition region, these changes are small (within 5%) as seen by the temperature dependence of the Mossbauer isomer shift (Fig. 8). Hence, the large reduction in the effective orbital/spin moment ratio cannot be attributed to improper sum-rules normalization due to uncertainties in hole occupation among the various Fe sites, and it is rather due to a strong variation in $3d$ orbital moment, as discussed below.

A nonzero value of m_{orb} is inconsistent with a half-filled $3d^5$ electronic state of Fe^{+3} ions. It was reported by Gich *et al.*[26] that among the four Fe sublattices present in ϵ-Fe_2O_3 nanoparticles two O_h (Fe_{DO1} and Fe_{DO2}) and the T_d (Fe_T) sites are distorted. Contrary to the other iron oxides which,
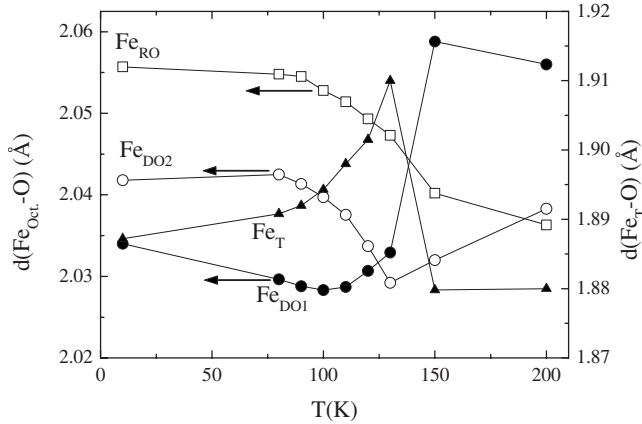
FIG. 6. Temperature dependence of the average Fe-O bond lengths, d, for the different Fe sites.

due to their crystalline symmetry, exhibit $m_{orb} \sim 0$, the distortions of Fe^{3+} coordination polyhedra observed in ϵ-Fe_2O_3 result in Fe $3d$-O $2p$ mixing and O $2p$ to Fe $3d$ charge transfer which, together with crystal-field effects, lifts the electronic degeneracy leading to a nonzero m_{orb}. Then, the mechanism at the high-temperature range ($T > 200$ K) should be similar to the one proposed by Kim *et al.*[35] and Arima *et al.*[39] for GaFeO$_3$ which is isostructural to ϵ-Fe_2O_3. Namely, the off-center displacement of the Fe ions along the c and b axes results in broken orbital parity symmetries and thus nonzero orbital moments, along the axes orthogonal to the displacement direction, i.e., (a and b) and (a and c), respectively. Since the largest hybridization is expected to be along c and the smallest along a, the largest orbital moment is found to be along a, which becomes the magnetic easy axis due to the spin-orbit coupling anisotropy energy. Based on the Bruno model and on the correlation between m_{orb}, and the magnetic anisotropy,[40,41] we can argue that the large m_{orb} at room temperature is the origin of the moderately large anisotropy found in this material. Moreover, a large spin-orbit coupling would explain the coupling of the magnetic and dielectric properties of ϵ-Fe_2O_3 reported in Ref. 25.

Similarly, the large reduction in m_{orb} at ~ 120 K, and the related weakening of spin-orbit interactions, is responsible for the decrease in the anisotropy constant at the collapse of H_C around ~ 110 K (Fig. 1). The origin of the m_{orb} instability can be correlated with a lattice distortion accompanying the commensurate to incommensurate magnetic transition of ϵ-Fe_2O_3. Indeed, Fig. 6 presents the temperature dependence of the average Fe-O bond lengths obtained from the joint Rietveld refinement of neutron and x-ray powder diffraction patterns between 10 and 200 K. As it can be seen, all the Fe sites present anomalies in their bond lengths but the Fe$_T$-O and F$_{DO1}$-O distances exhibit the largest anomalies in the temperature range where the minimum in m_{orb} occurs. Similarly, the temperature dependence of the different cell parameter ratios shows that a/c and b/c display a local maximum at ~ 130 K (see Fig. 7). Since no such anomaly is detected for a/b (the observed trends are within the error bars), it means that the c axis experiences an increased contraction as compared to a and b which can be related to the observed decrease in magnetocrystalline anisotropy via the m_{orb} dimi-
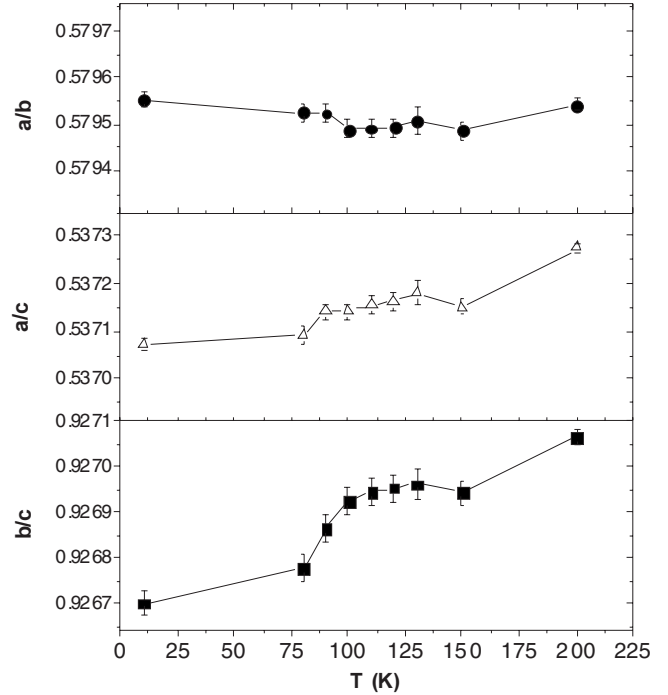

FIG. 7. Temperature dependence of unit cell parameter ratios.

nution. Interestingly, orbital moment instability has been previously reported in Nd$_2$Fe$_{14}$B at the spin reorientation transition temperature[42] and coinciding with a lattice distortion. Remarkably, the decrease in m_{orb} and the collapse of H_C in ϵ-Fe_2O_3 only take place in a limited temperature range. As discussed by Garcia *et al.*[42] for Nd$_2$Fe$_{14}$B, this implies that these effects are not so much related to the different low and high temperature magnetic phases but to the phase transition itself and the concomitant change in order parameter (e.g., Fe-O bond length in our case). It is interesting to note that the low-temperature (150–80 K) lattice distortion and the orbital moment instability described herein are not observed for the isostructural GaFeO$_3$,[35,39] where Ga atoms preferentially occupy sites equivalent to Fe$_T$ and Fe$_{RO}$ sites which are not distorted. This suggests that the lattice distortion is actually initiated by subtle changes in magnetic structure which cooperatively induce the lattice distortion through the spin-orbit coupling. Interestingly, the coercivity of ϵ-Fe_2O_3 begins to decrease just below 200 K (Fig. 2) concurrently with the intensity reduction in the (120) neutron powder diffraction magnetic reflection reported in Ref. 26. Moreover, the observed magnetic transition is in concordance with the well-known magnetic transitions in other Fe oxides taking place around 150–250 K [i.e., the Morin transition at $T_M = 260$ K in α-Fe_2O_3 (Ref. 43) and the Verwey transition at $T_V = 125$ K in Fe$_3$O$_4$ (Ref. 44)]. This implies that the magnetic coupling energies in ϵ-Fe_2O_3 should be of the same order of magnitude as in the other Fe oxides and substantially higher than in GaFeO$_3$. If we assume that the magnetism drives the lattice distortion, then the re-entrant behavior of the orbital instability can be qualitatively understood: a change in the magnetic structure induces a lattice distortion, through the spin-orbit coupling that exists due to a nonzero m_{orb}, but this
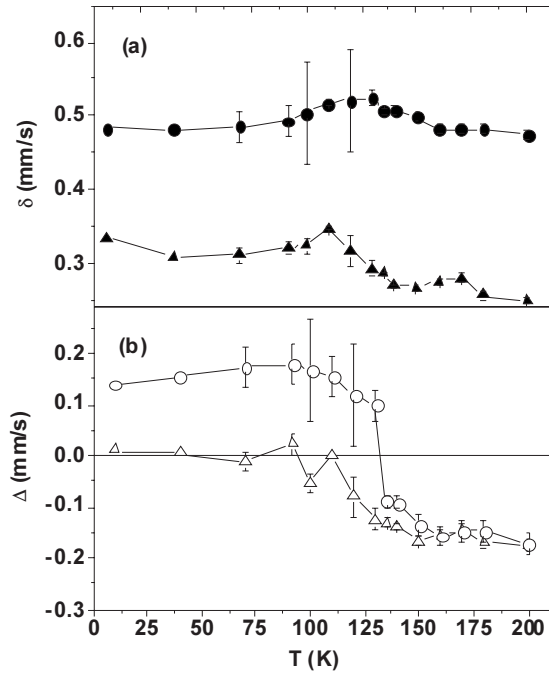
FIG. 8. Temperature dependence of Mössbauer spectral parameters for the Fe_{DO1} O_h site (circles) and the Fe_T T_d site (triangles) adapted from Ref. 26; (a) displays the dependency of the isomer shift (δ: filled symbols) and (b) the quadrupolar splitting (Δ: empty symbols).

distortion has in turn the effect of reducing m_{orb} and thus the distortion cannot be stabilized. Recent results from Mössbauer spectroscopy could provide additional hints to the origin of the large decrease in the orbital moment in ϵ-Fe$_2$O$_3$. A relationship between the Mössbauer isomer shift (δ) and the weight of charge transfer, and hence to covalency, has recently been established by Sadoc et al.,[45] giving a measure of the deviation from the formal charge rather than absolute charge. In particular, large positive shifts are expected for highly ionic complexes where the actual charge is very close to the formal ionic charge, while small and negative shifts would indicate strong deviations from the ionic model. The relatively small δ values reported for ϵ-Fe$_2$O$_3$ in Ref. 26 (between 0.3 and 0.5 mm/s relative to metallic Fe) support the notion of Fe $3d$-O $2p$ mixing. Interestingly, the temperature dependence of δ for the Fe_{DO1} O_h and the Fe_T T_d sites [see Fig. 8(a)] shows a maximum around 130 and 110 K, respectively, which, in the light of the work of Sadoc et al.,[45] can be related to the decrease in m_{orb} observed in the present work. The quadrupolar splitting (Δ), which is related to the electric field gradient, the quadrupolar moment of the Fe nuclei, and their relative orientation also present strong anomalies for Fe_{DO1} and Fe_T in that temperature interval [see Fig. 8(b)]. Namely, for Fe_{DO1}, Δ presents a sharp steplike change from -0.135 to $+0.167$ mm/s between 160 and 100 K, being zero around 130 K in coincidence with the mini-

mum in m_{orb}. For Fe_T, Δ gradually increases from -0.154 mm/s at 160 K to zero at about 110 K. The Fe_T and Fe_{DO1} coordination polyhedra lie in the same (001) planes and share corners through a common oxygen atom (O2 in Ref. 26) wherein significant Fe $3d$-O $2p$ mixing occurs. From the above discussion, the mechanism behind the reduction in m_{orb} and the coercivity collapse through a decrease in the spin-orbit interactions seems to be related to a reduction in charge transfer and the associated increased ionicity of the Fe_T-O2-Fe_{DO1} bonds at the transitional temperature range. Most likely, the changes in the electron transfer between the Fe_T and the Fe_{DO1} ions and the O2 ions arise from the significant change in Fe-O bond length by as much as 10%, according to the Rietveld refinements of x-ray and neutron diffraction patterns (see Fig. 6).

IV. CONCLUSIONS

We conclude that at room temperature, coordination polyhedra distortions for Fe_{DO1} and Fe_{DO2} observed in ϵ-Fe$_2$O$_3$ result in Fe $3d$-O $2p$ mixing and O $2p$ to Fe $3d$ charge transfer which, together with crystal field effects, lifts the electronic degeneracy leading to a nonzero m_{orb} resulting in a moderate anisotropy, a large coercivity, and magnetoelectric effects in this material. At the temperature range where the transition from the commensurate to incommensurate magnetic state begins, some lattice distortions were identified as responsible for the large reduction in m_{orb}, the related weakening of spin-orbit interactions, implying a decrease in the anisotropy constant and the collapse of H_C around $\sim$110 K. We argue that this decrease in orbital moment originates from the reduction in electron transfer between Fe and O ions for the Fe_T and Fe_{DO1} sites leading to an increase in the ionicity of some Fe-O-Fe bonds. m_{orb} shows a re-entrant behavior after the magnetic transition due to the nonmonotonic behavior of the Fe-O bond lengths.

*Corresponding author; haskel@aps.anl.gov

†Corresponding author; Marti.Gich@saint-gobain.com

‡Corresponding author; roig@icmab.es

[1] J. Jin, T. Iyoda, C. Cao, Y. Song, L. Jiang, T. Jin Li, and D. Zhu, Angew. Chem., Int. Ed. **40**, 2135 (2001).

[2] X. Teng, D. Black, N. J. Watkins, Y. Gao, and H. Yang, Nano Lett. **3**, 261 (2003).

[3] K. Woo, J. Hong, S. Choi, H.-W. Lee, J.-P. Ahn, C. S. Kim, and S. W. Lee, Chem. Mater. **16**, 2814 (2004).

[4] H. Kim, M. Achermann, L. P. Balet, J. A. Hollingsworth, and V. I. Klimov, J. Am. Chem. Soc. **127**, 544 (2005).

[5] B. Yang, Y. Wu, B. Zong, and Z. Shen, Nano Lett. **2**, 751 (2002).

[6] R. Hertel, W. Wulfhekel, and J. Kirschner, Phys. Rev. Lett. **93**, 257202 (2004).

[7] S. Chakraverty, M. Bandyopadhyay, S. Chatterjee, S. Dattagupta, A. Frydman, S. Sengupta, and P. A. Sreeram, Phys. Rev. B **71**, 054401 (2005).

[8] C. C. Wu, L. Y. Lin, L. C. Lin, H. C. Huang, Y. F. Yang, Y. B. Liu, M. C. Tsai, Y. L. Gao, W. C. Wang, S. W. Huang, S. Y. Yang, H. E. Horng, H. C. Yang, W. Y. I. Tseng, H. I. Yeh, C. F. Hsuan, T. L. Lee, and W. K. Tseng, Appl. Phys. Lett. **92**, 142504 (2008).

[9] M. Respaud, J. M. Broto, H. Rakoto, A. R. Fert, L. Thomas, B. Barbara, M. Verelst, E. Snoeck, P. Lecante, A. Mosset, J. Osuna, T. Ould Ely, C. Amiens, and B. Chaudret, Phys. Rev. B **57**, 2925 (1998).

[10] F. Bødker, M. F. Hansen, C. B. Koch, K. Lefmann, and S. Mørup, Phys. Rev. B **61**, 6826 (2000).

[11] S. Sahoo, O. Petracic, W. Kleemann, S. Stappert, G. Dumpich, P. Nordblad, S. Cardoso, and P. P. Freitas, Appl. Phys. Lett. **82**, 4116 (2003).

[12] J. Nogués, V. Skumryev, J. Sort, S. Stoyanov, and D. Givord, Phys. Rev. Lett. **97**, 157203 (2006).

[13] H. Forrestier and G. C. Guiot-Guillain, Acad. Sci., Paris, C. R. **199**, 720 (1934).

[14] R. Schrader and G. Büttner, Z. Anorg. Allg. Chem. **320**, 220 (1963).

[15] E. Tronc, C. Chaneac, and J. P. Jolivet, J. Solid State Chem. **139**, 93 (1998).

[16] J. Jin, S. Ohkoshi, and K. Hashmoto, Adv. Mater. (Weinheim, Ger.) **48**, 16 (2004).

[17] M. Popovici, M. Gich, D. Niznansky, A. Roig, C. Savii, L. Casas, E. Molins, K. Zaveta, C. Enache, J. Sort, S. de Brion, G. Chouteau, and J. Nogués, Chem. Mater. **16**, 5542 (2004).

[18] M. Gich, A. Roig, E. Taboada, E. Molins, C. Bonafos, and E. Snoeck, Faraday Discuss. **136**, 345 (2007).

[19] T. Nakamura, Y. Yamada, and K. Yano, J. Mater. Chem. **16**, 2417 (2006).

[20] S. Sakurai, J. Shimoyama, K. Hashimoto, and S. Ohkoshi, Chem. Phys. Lett. **458**, 333 (2008).

[21] M. Tadić, V. Spasojević, V. Kusigerski, D. Marković, and M. Remškar, Scr. Mater. **58**, 703 (2008).

[22] M. Gich, A. Roig, C. Frontera, E. Molins, J. Sort, M. Popovici, G. Chouteau, D. Martin y Marero, and J. Nogués, J. Appl. Phys. **98**, 044307 (2005).

[23] S. Sakurai, J. Jin, K. Hashimoto, and S. Ohkoshi, J. Phys. Soc. Jpn. **74**, 1946 (2005).

[24] M. Kurmoo, J. L. Rehspringer, A. Hutlova, C. D'Orleans, S. Vilminot, C. Estournes, and D. Niznansky, Chem. Mater. **17**, 1106 (2005).

[25] M. Gich, C. Frontera, A. Roig, J. Fontcuberta, E. Molins, N. Bellido, Ch. Simon, and C. Fleta, Nanotechnology **17**, 687 (2006).

[26] M. Gich, C. Frontera, A. Roig, E. Taboada, E. Molins, H. R. Rechenberg, J. D. Ardisson, W. A. A. Macedo, C. Ritter, V. Hardy, J. Sort, V. Skumryev, and J. Nogués, Chem. Mater. **18**, 3889 (2006).

[27] G. Burns, *Solid State Physics* (Academic, New York, 1985), p. 578.

[28] B. T. Thole, P. Carra, F. Sette, and G. van der Laan, Phys. Rev. Lett. **68**, 1943 (1992).

[29] P. Carra, B. T. Thole, M. Altarelli, and X. Wang, Phys. Rev. Lett. **70**, 694 (1993).

[30] C. T. Chen, Y. U. Idzerda, H. J. Lin, N. V. Smith, G. Meigs, E. Chaban, G. H. Ho, E. Pellegrin, and F. Sette, Phys. Rev. Lett. **75**, 152 (1995).

[31] J. W. Freeland, J. C. Lang, G. Srajer, R. Winarski, D. Shu, and D. M. Mills, Rev. Sci. Instrum. **73**, 1408 (2002).

[32] J. Rodríguez-Carvajal, Physica B **192**, 55 (1993).

[33] R. A. Brand, Nucl. Instrum. Methods Phys. Res. B **28**, 398 (1987).

[34] Independent of magnetization direction relative to the photon wave vector; here, assumed equal to $(\mu^+ + \mu^-)/2$, with $\mu^\pm$ absorption coefficients for opposite x-ray helicity of circular light, along and opposite the magnetization direction.

[35] J. Y. Kim, T. Y. Koo, and J. H. Park, Phys. Rev. Lett. **96**, 047205 (2006).

[36] M. Pilard, O. Ersen, S. Cherifi, B. Carvello, L. Roiban, B. Muller, F. Scheurer, L. Ranno, and C. Boeglin, Phys. Rev. B **76**, 214436 (2007).

[37] The substantial overlap of the L_2 and L_3 edges in Fe can lead to errors in the spin sum rule, which depending on the crystal field might be up to 50%; F. de Groot (unpublished).

[38] Since the electron sampling depth of TEY in oxides is typically a few nanometers and the radius of the nanoparticles is 12.5 nm, the measurements could suffer from enhanced surface sensitivity; K. Fauth, Appl. Phys. Lett. **85**, 3271 (2004).

[39] T. Arima, D. Higashiyama, Y. Kaneko, J. P. He, T. Goto, S. Miyasaka, T. Kimura, K. Oikawa, T. Kamiyama, R. Kumai, and Y. Tokura, Phys. Rev. B **70**, 064426 (2004).

[40] P. Bruno, Phys. Rev. B **39**, 865 (1989).

[41] P. Gambardella, S. Rusponi, M. Veronese, S. S. Dhesi, C. Grazioli, A. Dallmeyer, I. Cabria, R. Zeller, P. H. Dederichs, K. Kern, C. Carbone, and H. Brune, Science **300**, 1130 (2003).

[42] L. M. García, J. Chaboy, F. Bartolomé, and J. B. Goedkoop, Phys. Rev. Lett. **85**, 429 (2000).

[43] D. Schroeer and R. C. Nininger, Phys. Rev. Lett. **19**, 632 (1967).

[44] F. Walz, J. Phys.: Condens. Matter **14**, R285 (2002).

[45] A. Sadoc, C. De Graaf, and R. de Boer, Chem. Phys. Lett. **126**, 13470 (2008).